Published in IET Electric Power Applications
Received on 18th October 2013
Revised on 19th December 2013
Accepted on 20th January 2014
doi: 10.1049/iet-epa.2013.0330

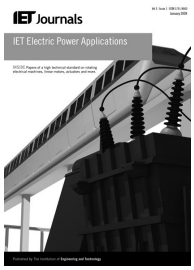

ISSN 1751-8660

Time-domain finite-element technique for quantifying the effect of sustained ferroresonance on power transformer core bolts

Charalambos A. Charalambous[1†], Zhongdong Wang[1], Paul Jarman[2], Jonathan Peter Sturgess[3]

[1]*School of Electrical and Electronic Engineering, University of Manchester, Manchester M13 9PL, UK*
[2]*National Grid, Warwick Technology Park, Warwick CV34 6DA, UK*
[3]*Alstom Grid Research and Technology, Stafford ST17 4LX, UK*
E-mail: zhongdong.wang@manchester.ac.uk
[†]*Present address: Department of Electrical and Computer Engineering, University of Cyprus, Nicosia, Cyprus*

Abstract: Detailed investigation of the effects of ferroresonance on power transformers requires a method that is able to quantitatively and topologically assess the core saturation and the stray fields attributed to flux redistribution. This study describes a time-domain finite-element approach to model a ferroresonance condition and quantify its effect. More specifically the model generates sustained ferroresonance waveforms and, crucially, also allows examination of the effect of the resulting high core fluxes on the transformer core clamping bolts. Two benchmarking concepts are used to aid this: (i) the space-averaged permeability variation and (ii) a topological calculation of flux variation within the core.

1 Introduction

The UK transmission network is a highly integrated system, containing many double circuit lines terminating, in some cases, with mesh design substations. During the 1970s, when the transmission network was built, the prohibitively high cost of circuit breakers drove the development of the mesh substation. As a consequence, a number of power transformers are exposed to ferroresonance where they are connected to mesh corner and circuit tee configurations. UK experience [1] suggests that one in ten circuit de-energisation can be driven into ferroresonance, the probability depending upon the appropriate initial conditions being established. It is believed that ferroresonance is a contributing factor to the eventual failure mode by exposing the transformer's components to electromagnetic and thermal stresses. The impact on these components is mainly associated with accelerated ageing and can be estimated through the power dissipated through Ohmic heating in the structural parts of the transformer (e.g. flux shunts and core frames).

Furthermore, many of the older transformer cores on the UK system are clamped with tie bolts. There is a consequent concern that the overfluxing of the core that takes place during ferroresonance could give rise to substantial eddy current heating of the core bolts, causing damage to the core bolt insulation systems and leading to internal short-circuits within the core. It is, therefore, desirable to be able to identify the regions of the core that are most susceptible, and to evaluate the heating effect especially where magnetic core bolts were used in the construction of the core. A decision can then be made as to whether remedial action is required.

Investigation of the ferroresonance phenomenon is characterised by two main approaches. The first is to make experimental field tests on suitable circuits that can be induced to resonate [2]. This approach provides a realistic appreciation of the magnitude and the frequency (mode) of the associated overvoltages and overcurrents as well as quantifying the effect on switchgear because of the de-energisation of a power transformer attached to a long overhead line circuit.

However, the physical size of the associated power equipment enforces logistic and other security/safety/cost-related restrictions on large-scale experiments and testing, particularly if the core is to be instrumented. Therefore it is prudent for engineers to adopt a second approach that utilises detailed mathematical models for computer transient simulations of the system. This approach has the advantage of enabling the assessment of the likelihood of ferroresonance occurrence, and the stresses that it imposes, for a number of network configurations [3, 4].

The majority of the existing simulation practices are based on equivalent circuit models which describe, to an extent, the interaction of the power system components with the transformer model in the event of ferroresonance. A comprehensive literature on the ferroresonance phenomenon with the associated simulation models is given in [5–8]. The modelling of ferroresonance behaviour through an appropriate hysteresis model is addressed in [9], whereas

specific details on fundamental mode ferroresonance are documented and explained in [10]. A laboratory-based investigation of the phenomenon is given in [11].

Nevertheless, existing modelling approaches lack the ability to provide an insight into the flux distribution and redistribution, under transient conditions, within the transformer's complex structure. The latter is of significant importance especially in the case of high-magnitude ferroresonant currents that give rise to a high magnetomotive force (MMF), which not only corresponds to core saturation but also causes flux to leak from the core and penetrate other structural parts of the transformer. The finite-element method is applicable to this type of calculation and can be utilised to quantitatively and topologically assess the saturation of the core (and other structural parts), arising from such a flux redistribution. The finite-element technique can model the true geometry of the transformer in two and three dimensions (2D and 3D) and can account for the induced currents in complex-shaped components. Non-linear characteristics of materials are allowed for through iterative methods, and non-sinusoidal time variation may be handled by time-stepping techniques [12].

One concern, when dealing with finite-element modelling, is the interface between the electrical power system components and the transformer finite-element model itself. A considerable research activity has been noted in the literature considering the coupling of magnetic and electric circuit equations in the analysis of electromagnetic systems [13–15]. For example, Dreher and Meunier [13] describe a frequency-domain simulation with the finite-element transformer model coupled to electric circuit equations consisting of a simple Thevenin equivalent voltage source and impedance.

Nevertheless, there is a room for extending the external electrical circuit representation, especially when it comes to modelling the interaction of power systems with power transformers, as the system capacitances are critical to the initiation and maintenance of ferroresonance.

The aim of this work is to provide a simpler technique to look at the core overfluxing and its consequence for the transformer's structural components. Therefore a model is developed to obtain a ferroresonance condition and subsequently to examine the effect of the resulting high core fluxes on the transformer core clamping bolts through the concepts of the time-varying space-averaged permeability and a topological calculation of the flux variation within the core.

2 Definition of the problem

When using the finite-element method to provide transient electromagnetic field calculations (e.g. for ferroresonance) for large power transformers, the winding current is needed as the input quantity to the corresponding finite-element model [16]. In some cases the winding current can be obtained either directly by field measurements or indirectly, by the use of equivalent circuit based transient simulation software that is qualified for these calculations.

However, acquiring suitable real-scale test results during switching operations, especially on 400 kV system networks, is difficult, because they are very rare, and those that are undertaken are rarely reported [1, 17]. Furthermore, the resolution of available ferroresonance field measurements of voltage and current at the 400 kV level may be insufficient for use directly in the finite-element calculation. Sometimes, however, these measurements can be used as inputs to an equivalent circuit-based simulation of the ferroresonance condition, whose output can be specified to be detailed enough to be suitable for use in subsequent finite-element calculations.

Where these types of equivalent circuit-based techniques are used to calculate the input current for the finite-element model, a compatibility validation of the two transformer models (f.e. and equivalent circuit) should be carried out. The principle of the validation is to compare the measured voltage waveform (used as input data to the circuit-based model) with the voltage waveform produced as an output from the finite-element model to verify that the two are consistent. This validation ensures that the flux distribution within the core of the finite-element model is represented accurately.

However, there may simply be no measured data for the case to be studied, and compatibility validation is not always feasible because the analytical and finite-element models may have different parameters (e.g. representation of core saturation). To cope with this, an autonomous modelling approach is used here that encompasses not only the evaluation of the transformer's ferroresonance-related effects but also the generation of ferroresonance waveforms, all within a single numerical model. The aim of this approach is to assume as input only a set of balanced three-phase system voltages and to combine this with appropriate representations of the transformer and transmission line.

Both 2D and 3D f.e. models of the transformer fields may be coupled with the circuit equations used to model the transmission system [13–15]. However, 3D f.e. models having the necessary level of detail to allow examination of localised field effects are rarely affordable for problems requiring solution in the time domain, such as ferroresonance modelling. Consequently, the main analysis in this paper has used a 2D time-domain solver within SLIM [18], which handles within the one package, the definition and integration of the circuit equations with the field equations.

3 Model

The modelling is carried out on a 1000 MVA 400/275/13 kV autotransformer, for which fundamental ferroresonance field test recordings are available [2]. The recordings are of a number of switching tests on a circuit configuration which was known to exhibit ferroresonance. Specific test details are given in [19].

3.1 Finite-element transformer model

Fig. 1 shows a cross-section of the finite-element model of the transformer to be studied. The physical dimensions of the structures: core, limb and yoke, winding, insulation clearance and other structural parts were taken from the manufacturer's design data sheets. Table 1 gives the principal core dimensions.

The transverse view of Fig. 1 has been employed in the 2D analysis of this paper, as it can establish the level of core saturation under ferroresonance conditions by explicitly representing the flow of flux from limb to limb and from phase to phase. The 2D model incorporates a 'core depth' factor (defined as the ratio of the core's area to its diameter) to ensure that there is the correct amount of flux in the

doi: 10.1049/iet-epa.2013.0330

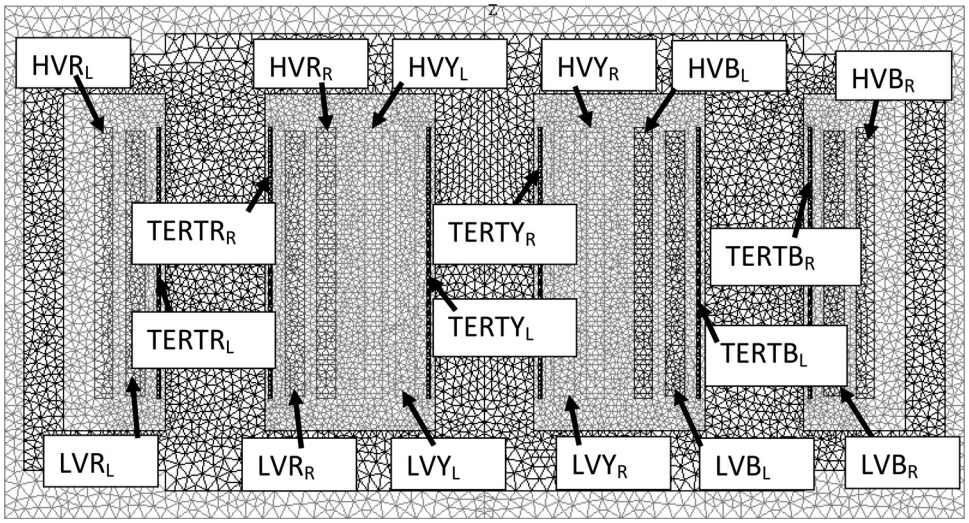

Fig. 1 *2D Finite-element mesh for an autotransformer*

model and for use as a multiplying factor in the voltage calculation.

The three windings present in the model are (taken outwards from the core) the tertiary, the common (low voltage) and the series (high voltage) winding, Fig. 1. Each winding is modelled in two parts, that is, the 'go' (left) side of the winding and the 'return' (right) side of the winding (e.g. HVR_L and HVR_R). The current in these regions, and the electromotive force (emf) induced by the fields in the coils that they represent are the point of linkage between the finite-element model and the power system network model.

3.2 Power system network characteristics

Fig. 2 illustrates a single-line diagram of the circuit arrangement that is modelled. The length of the parallel overhead line circuit is ~37 km and the feeder has a 1000 MVA 400/275/13 kV SGT_1 power transformer, for which the ferroresonance field recordings are available.

The transmission line network contains a double circuit of three-phase two-bundle conductors, the details of which are given in Table 2 and Fig. 2. The spacing between the conductors of the bundle is 50 cm and the phases are labelled as *R* (Red), *Y* (Yellow) and *B* (Blue).

Table 1 Core dimensions

core diameter	800 mm
distance between phase centres	1694 mm
unwound phase centres	1115 mm
leg length	2720 mm
yoke diameter	480 mm
outer yoke diameter	320 mm

4 Description of the methodology

The network configuration presented in Section 3 is a susceptible circuit that could be induced to resonate. When side A of the double circuit transmission line connected to the transformer SGT_1 is switched out, see Fig. 2, the energised adjacent line (side B) is capable of supporting an established ferroresonance condition which may arise between the non-linear core inductance of the transformer SGT_1 and the circuit capacitance to ground of the de-energised line.

The sequence of switching conditions and operations were as follows: At the 400 kV side the disconnector X_{303} was locked open and mesh corner 3 restored to service. At the 275 kV side the circuit breaker T_{10} is open. At the 400 kV all disconnectors and circuit breaker X_{420} are in service. Point-on-wave (POW) switching was carried out on the circuit using circuit breaker X_{420} to induce ferroresonance. This type of switching prevents switching overvoltage conditions and provides a degree of controllability to the tests. The circuit breaker was tripped via an external POW control device.

Thus, Fig. 3*a* illustrates the equivalent circuit that describes the capacitive coupling between the two circuits as well as the circuits' capacitance to ground, per phase, following the switching operations. A simplified version of the circuit

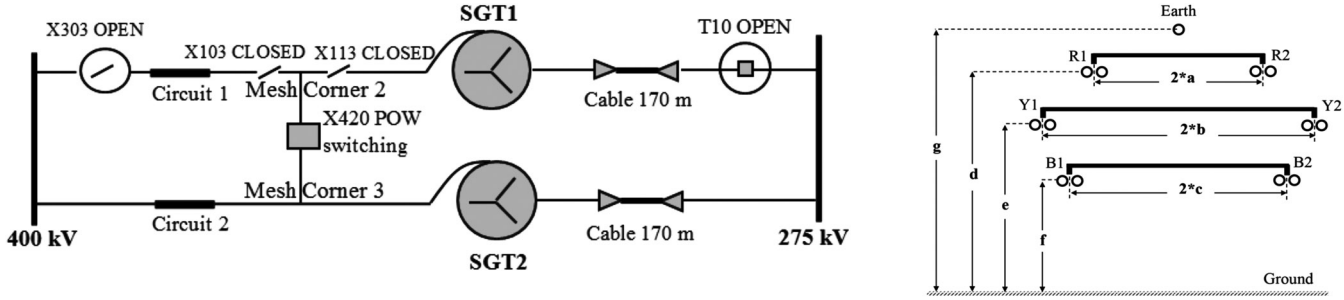

Fig. 2 *Single-line diagram of the circuit arrangement and design topology of tower – 400 kV network*

Table 2 Tower and transmission line characteristics

Conductor dimensions (including sag) for O.H.L. design						
Tower design L6/2		Operational voltage 400 kV		Insulation voltage 400 kV		
a, m	*b*, m	*c*, m	*d*, m	*e*, m	*f*, m	*g*, m
6.93	10.16	8.33	33.5	23.03	14.19	44.04

Conductor parameters						
	Material	Outer radius, mm	Outer diameter, mm	ac resistance, Ω/km	No. of strands	Resistivity, μΩm
phase	AAAC	18.63	37.26	0.04	61	0.0312
earth	AACSR	9.765	19.53	0.1654	30/7	0.0295

(see Fig. 3*b*) is sourced by three-phase sinusoidal voltages and is linked to the windings of the transformer taking into account the core's non-linearity.

Specifically, the transformer finite-element model of Fig. 1 is associated with the modelled external electrical circuit (Fig. 3*b*) via the windings (HVR_L, HVR_R etc.) as shown in Fig. 4.

The windings of the transformer (see Fig. 1) are assumed to be sufficiently finely stranded and transposed that the eddy currents induced in them are negligible. The tertiary winding is modelled as a separate, isolated delta-connected entity, enabling currents to be induced in it by the calculated fields. It is crucial to include this winding in the model as a tertiary winding on a five-limb core will drastically alter the zero sequence impedance by allowing zero sequence currents to circulate around the delta tertiary winding and thus balance those flowing into the primary winding.

The transformer is modelled to represent the condition of the core prior to the establishment of the ferroresonance event (i.e. before the transformer 'sees' the capacitive network). This is achieved by specifying the core's initial

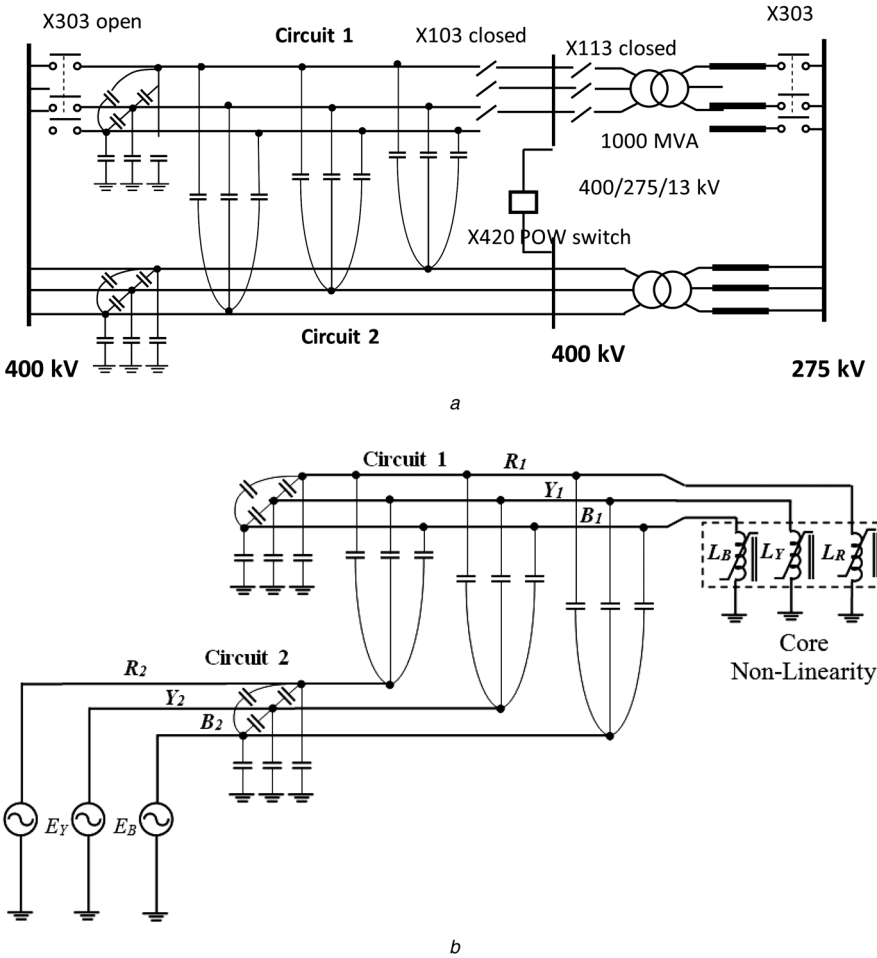

Fig. 3 *Equivalent circuit with the capacitive coupling for which the resonance condition is established*

a Equivalent circuit with the capacitive coupling for which the resonance condition is established
b Simplified equivalent circuit with the capacitive coupling for which the resonance condition is established

doi: 10.1049/iet-epa.2013.0330

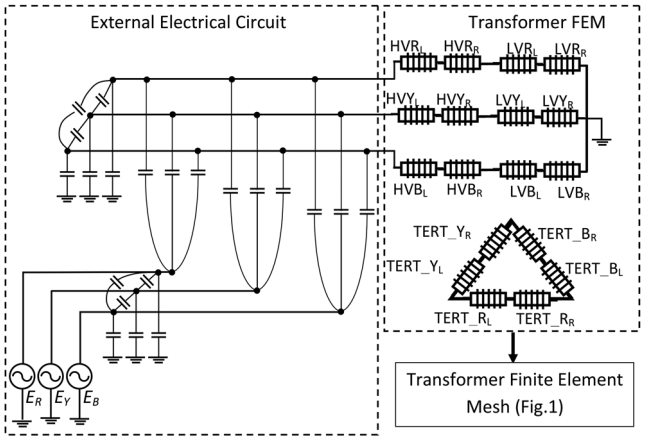

Fig. 4 *Equivalent electrical circuit integrated with the finite-element transformer model (Fig. 1)*

permeability distribution to be that of the pre-ferroresonance steady-state condition. The solution of the ferroresonance problem is subsequently initiated from this preset core state. This approach eliminates any inrush-related phenomena in the model that could interfere with the calculated ferroresonance response.

4.1 Capacitance calculation

The transmission line described above consists of a double circuit with two conductors per phase, one earth aerial conductor and the earth itself. It constitutes a complicated system, with capacitances between pairs of conductors and capacitances between line conductors and earth.

The capacitance values of the circuit illustrated by Fig. 3 were derived from first principles by considering the charge and the potential of each conductor, assuming that all conductors are initially uncharged. In reality, the conductors may be charged but this will only influence the initial transient period of ferroresonance response. As the scope of this work is to establish a sustained mode of ferroresonance in order to assess its effects on the various parts of the transformer, the effect that an initial charge of the conductors may have on the establishment of a ferroresonance response may be neglected.

Hence, the relationship of the conductors' charge/capacitance to the conductors' voltage can be described with the use of the Maxwell coefficient matrix [20]. Thus, a corresponding capacitance matrix is deduced (1) reflecting on the geometrical arrangement of the conductors and the earth plane (see Fig. 2 and Table 2). The earth conductor is assumed to have zero potential. The diagonal elements of the capacitance matrix reflect the sum of capacitances per unit length of all elements connected to a particular node (see Fig. 3). The off-diagonal elements consist of the negative shunt capacitance per unit length between any two conductors. (see (1))

The calculated capacitance values are then entered into the model described by Fig. 4, taking into consideration the effective length of the transmission line network (37 km).

It was found that the simulated response is very sensitive to the capacitance values used in the model. Sensitivity studies showed that a $\pm 0.01\%$ change in the coupling capacitance values (i.e. the capacitances that connect the energised with the de-energised circuit), resulted in different ferroresonance responses such as chaotic and quasi-periodic. This is a well-known feature of ferroresonance. It should also be noted that the calculation of the capacitance is not accurate to 0.01%, because of discrepancies between the actual physical dimension of line and layout and the design values and to the fact that the distributed capacitance of the system is modelled by a lumped-parameter equivalent circuit. The calculated coupling capacitance values were adjusted by trial and error until a sustained ferroresonance response occurred. It was found that a change of 0.015% was required, a change that is smaller than the error incurred in modelling the transmission line by the simple, lumped-parameter equivalent circuit. This adjustment indicates the sensitivity of establishing the response with respect to the initial conditions of the test configuration [11].

4.2 Finite-element modelling specifics

Although modelling chaotic and sub-harmonic ferroresonance behaviour requires an appropriate hysteresis model [6], under fundamental mode ferroresonance, the transformer is forced to operate in the saturated region of its core characteristics. Therefore a single-valued representation of the core magnetic characteristics can be justified especially for fundamental mode ferroresonance [10].

Ferroresonance puts the transformer core into a highly saturated state and the magnetic field in the core in these conditions is well beyond the maximum value for which steel manufacturer's B–H data are available. To cater for

$$\begin{bmatrix} C_{R_1}+C_{R_1Y_1}+C_{R_1B_1} & -C_{Y_1R_1} & -C_{B_1R_1} & -C_{R_2R_1} \\ -C_{R_1Y_1} & C_{Y_1}+C_{Y_1R_1}+C_{Y_1B_1} & C_{B_1Y_1} & -C_{R_2Y_1} \\ -C_{R_1B_1} & -C_{Y_1B_1} & C_{B_1}+C_{B_1R_1}+C_{B_1Y_1} & -C_{R_2Y_1} \\ -C_{R_1R_2} & -C_{Y_1R_2} & -C_{B_1R_2} & C_{R_2}+C_{R_2Y_2}+C_{R_2B_2} \\ -C_{R_1Y_2} & -C_{Y_1Y_2} & -C_{B_1Y_2} & -C_{R_2Y_2} \\ -C_{R_1B_2} & -C_{Y_1B_2} & -C_{B_1B_2} & -C_{R_2B_2} \end{bmatrix}$$

$$\begin{bmatrix} -C_{Y_2R_1} & -C_{B_2R_1} \\ -C_{Y_2Y_1} & -C_{B_2Y_1} \\ -C_{Y_2B_1} & -C_{B_2B_1} \\ -C_{Y_2R_2} & -C_{B_2R_2} \\ C_{Y_2}+C_{Y_2R_2}+C_{Y_2B_2} & -C_{B_2Y_2} \\ -C_{Y_2B_2} & C_{B_2}+C_{B_2R_2}+C_{B_2Y_2} \end{bmatrix} \quad (1)$$

this, the *B–H* curve has to be extrapolated. Various methods are available [21] but all are, essentially, an approximation to the true (but unknown) behaviour, and all can give rise to flux densities that are higher than 'expected' [22]. For this work, a simple hand extrapolation to a final slope of μ_0 was used.

To incorporate the effect of the core 'build factor' (i.e. to allow for the small air gaps inevitably present at the joints between the yokes and limbs), the *B–H* curve for the core material (27m4) was scaled in the *H* dimension so that it became representative of the core as a whole, not just of the steel lamination material. The scaling factor was adjusted so that the core draws the correct magnetising current at 1 pu volts, open-circuit. This is, effectively, the method used by equivalent circuit-based models.

The windings are treated as current sources since they redistribute the current resulting from the equivalent circuit-based model (see Fig. 4). The winding flux linkage is calculated by utilising the vector magnetic potential $\boldsymbol{A}$, expressed in Wb/m as detailed in [23]. Then, the Poisson formula (2) in 2D for magnetic vector potential in terms of the winding current density J, the material properties (μ) and the variation through space is utilised. This formula is solved in numerical form by the circuit-coupled finite-element method.

$$J_z = -\left[\frac{\partial}{\partial x}\left(\frac{1}{\mu_o \mu_{\mathrm{r}}}\frac{\partial A_z}{\partial x}\right) + \frac{\partial}{\partial y}\left(\frac{1}{\mu_o \mu_{\mathrm{r}}}\frac{\partial A_z}{\partial y}\right)\right] \tag{2}$$

The equations for the power system are derived from a standard loop formulation, where the unknown variable is the loop current and Kirchhoff's voltage law is applied round each loop. Where the loop includes a transformer winding, the winding's emf is written in terms of the rate of change of the flux linkage with the winding, which can be related directly to the magnetic vector potential of the f.e. solution. The loop current may also be related to the winding current density, J_z. When the finite-element method is applied to (2) and combined with the loop equations written in matrix form and the forward Euler method for the discretisation in time, the result is (3), which is derived from [14] and the references contained therein.

$$\begin{bmatrix} [\boldsymbol{S}] & -[\boldsymbol{B}][\boldsymbol{D}]^{\mathrm{T}} \\ -[\boldsymbol{D}][\boldsymbol{B}]^{\mathrm{T}} & -\delta t[\boldsymbol{R}] - [\boldsymbol{L}] \end{bmatrix} \begin{pmatrix} (\boldsymbol{A}) \\ (\boldsymbol{i}) \end{pmatrix}_{t+\delta t} = \begin{pmatrix} (0) \\ -\delta t(\boldsymbol{U})_{t+\delta t} - [\boldsymbol{L}](\boldsymbol{i})_t - [\boldsymbol{D}][\boldsymbol{B}]^{\mathrm{T}}(\boldsymbol{A})_t \end{pmatrix} \tag{3}$$

where the stiffness matrix $[\boldsymbol{S}]$ expresses the finite-element equations, (2), $[\boldsymbol{R}]$ and $[\boldsymbol{L}]$ are matrices of circuit resistances and inductances, $[\boldsymbol{B}]$ is a connection matrix that relates loop currents to branch currents, $[\boldsymbol{D}]$ is a matrix that relates the vector potential solution and the number of turns in a winding to the flux linkage with the winding, $(\boldsymbol{i})$ is a vector of loop currents, $(\boldsymbol{A})$ is a vector of the magnetic vector potential, $(\boldsymbol{U})$ is a vector of source voltages and the voltages across the circuit capacitances ($(1/C)\int_0^t I_c \mathrm{d}t$) and δt is the time step length.

The non-linearity of the magnetic core is reflected in the fact that the coefficients of the stiffness matrix, $[\boldsymbol{S}]$, are dependent on the vector potential solution, $(\boldsymbol{A})$. A Newton–Raphson scheme is used to resolve the consequent non-linearity in (3). By this means, the field and the circuit equations are solved simultaneously, avoiding the need for repeated iteration between them, which could be very prone to non-convergence where there are large and rapid swings in core inductance. Stacking factors are utilised to model the effect of the lamination of the core by modifying the permeability values [24]. The resulting directional permeabilities will not significantly influence the leakage flux although, if they are ignored, this will give a pessimistic result [25]. Ferroresonance is a low-frequency effect; therefore the eddy current losses within the core may be neglected. On a final note, the finite-element model had 18 033 nodes and 35 846 elements. The problem was solved on a standard P.C. The time step length used in the simulation was 0.1 ms and each time step took about 10 s to evaluate.

5 Calculations and indirect validation of the model

The aim of this work is to look at the core overfluxing and its consequence for the transformer's structural components. However, no measurements of core or leakage flux are available to validate this aspect of the model, so it is necessary to make an indirect validation. It can be argued that if the predicted terminal current and voltage waveforms are close to those measured, then the core flux must be similarly accurate.

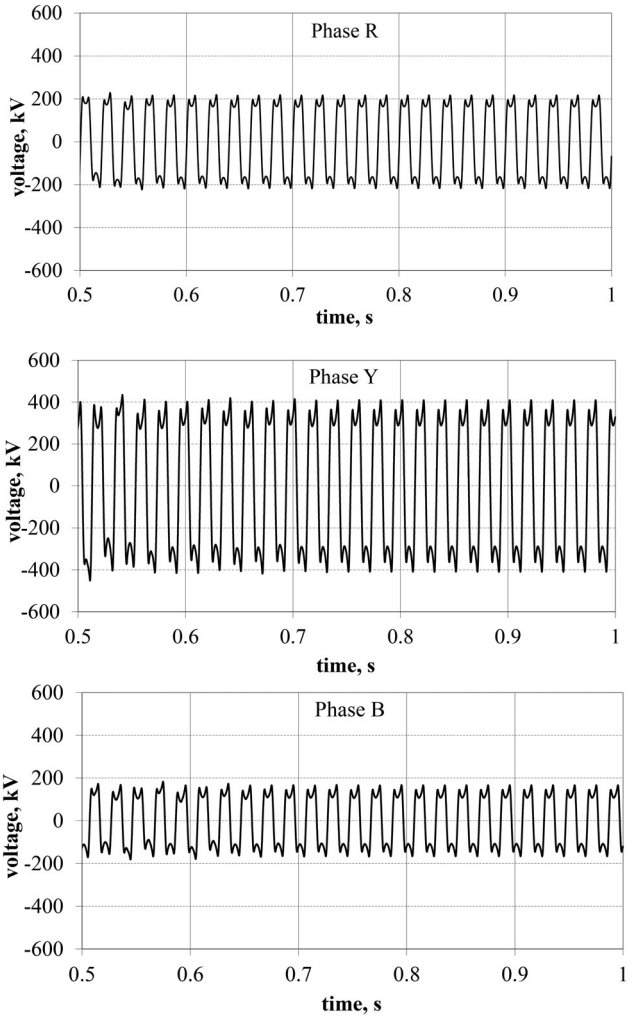

Fig. 5 *Simulated fundamental mode ferroresonance response – voltage*

doi: 10.1049/iet-epa.2013.0330

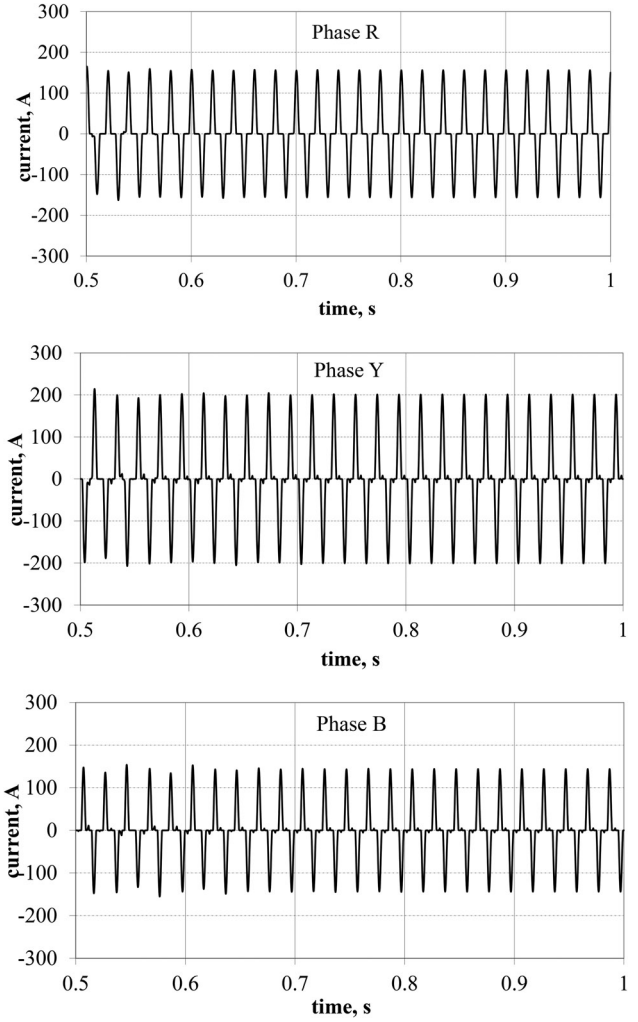

Fig. 6 *Simulated fundamental mode ferroresonance response – current*

To this end direct validation could, in principle, be made using measurements on a scale model although, as skin effect does not scale in the same way as other dimensions, this would not be a full validation. Nevertheless, future work could usefully include tests made on carefully designed scale models.

Figs. 5 and 6 illustrate the calculated ferroresonant voltages and currents, from 0.5 to 1 s of the simulation. The busbar voltage for the simulation was at 1 pu. The voltages shown in Fig. 4 are phase-neutral for which the per-unit base is 327 kV (peak).

The magnitude of the voltages is close to 1 pu (in contrast to chaotic modes of ferroresonance, where there are significant overvoltages >1.2 pu). However, UK experience [1] suggests that the sustained fundamental mode of ferroresonance is the most severe case because of the high energy transferred to the transformer. Phases *R* and *B* are in anti-phase with phase *Y*, suggesting that all the three-phase limbs would become highly saturated at the same instant. The current is several orders of magnitudes higher than the open-circuit magnetising current.

Fig. 7 compares the simulated waveforms with the field recordings for two periods of the phase *R* voltage and current waveforms, respectively. It is important to note, when studying the results, that the ferroresonance currents do not form a balanced, three-phase set – that is, the zero sequence current $3I_0$ is not equal to zero. The measured zero sequence current has a dominant third harmonic component and a maximum peak value of 36 A. A similar value is obtained when the simulated three-phase currents are summed.

This suggests that the dominant harmonics of ferroresonance response, that is, first, third, fifth, are represented adequately for the purpose of this work as is evident in Fig. 8, which is to evaluate overfluxing of the core that takes place during ferroresonance and which could cause damage to insulation systems because of the heating of core bolts by the eddy currents arising from the stray fields. The discrepancy between the field and simulated results is believed to be a result of uncertainty in the representation of the core's magnetisation in extreme saturation. As noted above, the simulation results are very dependent on the accuracy of the *B–H* curve employed at high flux densities. Since no field or laboratory measurements are available to determine the shape of the *B–H* curve at flux densities higher than 1.95 T, it is necessary to rely on extrapolation. However, it is the shape of the *B*/*H* curve, particularly in the very highly saturated region, that will determine the harmonic content of the ferroresonance response. Therefore the difference observed in the harmonic contents between field and simulation results may be because of the fact that the theoretical extrapolations performed by the software may deviate from the actual field conditions of the core's non-linearity.

However, the figures show that the simulated results are comparable with the recorded voltage and current waveforms. Consistent results were also obtained for phases

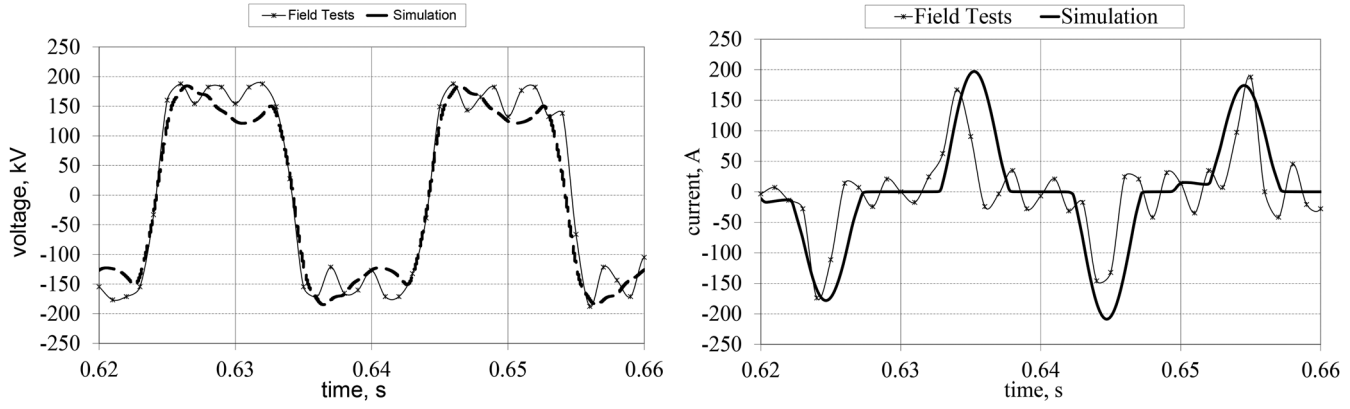

Fig. 7 *Comparison of phase R ferroresonance waveforms*

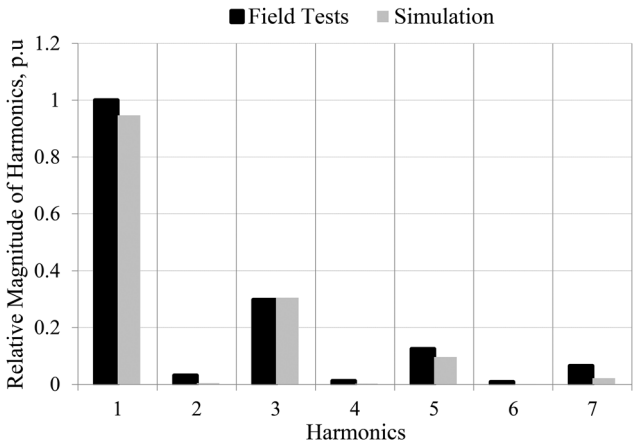

Fig. 8 *Relative comparison of dominant harmonics of voltage ferroresonance waveforms*

Y and *B*. From this, it may be inferred that the simulated core flux is a good representation of the actual flux in the core of the transformer under test. Although the higher harmonics of the response are less accurately calculated, they do not contribute significantly [26] to the core bolt heating effect, which is the subject of the present analysis.

6 Core susceptibility to sustained ferroresonance

Equivalent circuit-based methods for simulating ferroresonance are, also, able to generate terminal voltage and current waveforms, and can do so with much less computational effort. However, the developed methodology described in Section 4 can provide valuable visual evidence of the core state under saturating conditions topologically, enabling those regions most severely stressed to be identified.

As a general rule, f.e. simulations of power transformers are made in 3D in order to capture all the detail of the leakage fields. However, the present calculation can be performed with reasonable accuracy in 2D, since it principally concerns the core where the field distribution varies significantly only in the plane of the laminations (i.e. in the plane illustrated by Figs. 1 and 9). In the third direction, perpendicular to the laminations, the field does not change much; therefore neither does the permeability which in consequence shows a variation in only 2D.

Fig. 9 illustrates a snapshot of the flux density distribution which corresponds to the worst saturating conditions, reflecting on the waveforms presented by Figs. 5 and 6. Instantaneously and periodically (in a 50 Hz cycle), parts of the core achieve a flux density of 2.2 T during the ferroresonance event modelled although this absolute value is dependent on a theoretical extrapolation of the *B–H* curve at high flux densities (see Section 4.2).

Fig. 9 also illustrates core tie bolts in typical locations of the main limb area and the yoke areas which may be present in older transformer designs. These bolts are usually made of mild steel BS-4360, 20 mm in diameter.

To determine, by visual inspection of flux density plots, the instant in time at which the core was most saturated would be a time-consuming process, hence to aid investigation of the susceptibility of the core structure under sustained ferroresonance conditions, the concept of the space-averaged permeability variation was developed: low permeability being an indication of high saturation.

6.1 Space-averaged core permeability

The space-averaged value of the core's permeability (μ) at each time step in the time domain solution is found from a simple area-weighted average of the permeability of each element representing the core in the 2D mesh at that particular instant in time, (3). This concept was introduced in [25] for frequency-domain calculations, here it is extended into the time domain.

$$\overline{\mu_{\text{av}}}(t) = \frac{\sum_{i=1}^{n} \left[\Delta_i \times \mu_\iota(t)\right]}{\sum_{i=1}^{n} \Delta_i} \tag{4}$$

where Δ_i is the area of the ith element.

Fig. 10 illustrates the space-averaged permeability variation for the centre main limb, the right outer limb and the upper yoke. It clearly demonstrates that the lowest space-averaged permeability, which represents the highest core saturation, lies with the main limbs of the core. Moreover, the main

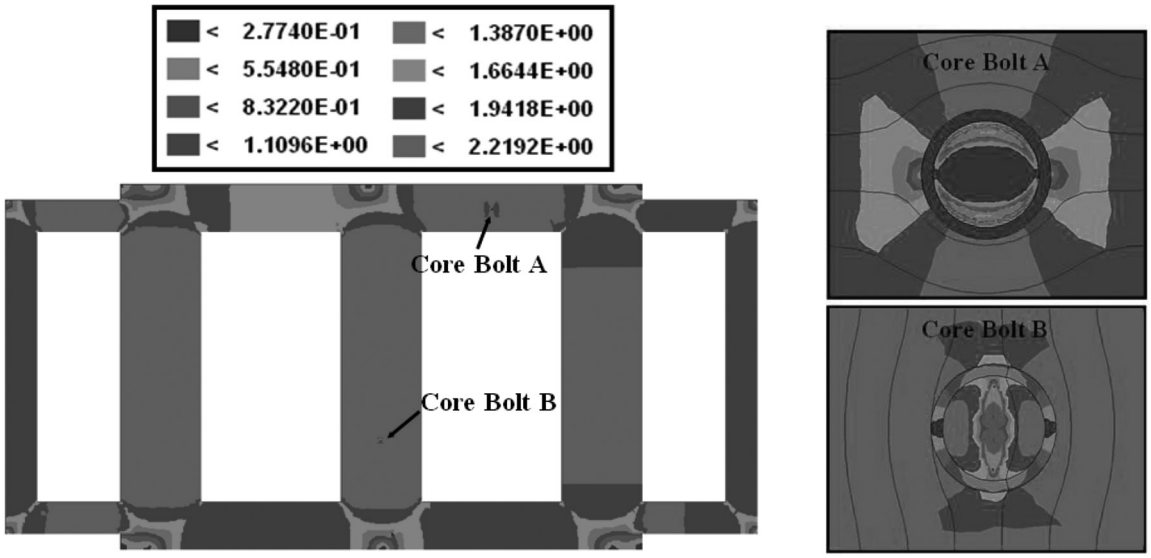

Fig. 9 *Instantaneous flux density distribution (tesla) – reflecting the time step of worst saturating conditions*

doi: 10.1049/iet-epa.2013.0330

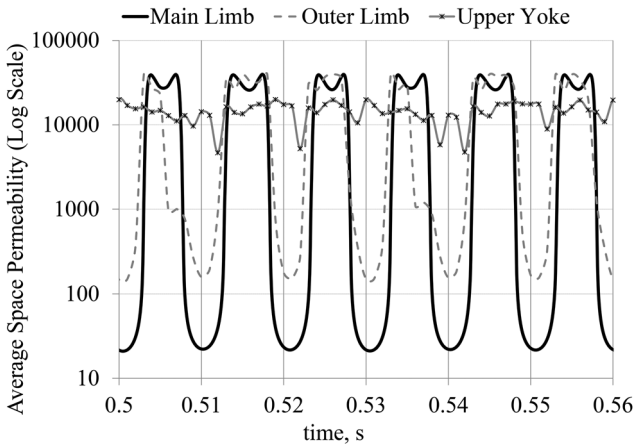

Fig. 10 *Space-averaged permeability variation – by core section*

limb structure maintains this low permeability value for a longer time, meaning that flux will tend to leak from the core steel for a longer proportion of each cycle.

It is evident that the space-averaged permeability distribution of the yoke structure is higher, implying that the saturation at that particular area is less severe (this is because a certain amount of flux, no longer confined to the limbs by the presence of the winding, can leak into the core window and bypass the yoke). It is also interesting to note that Fig. 9 reveals that the main limbs and outer limbs of the core reach their peak saturation level simultaneously, under this particular fundamental mode ferroresonance. This assessment is particularly important in older transformer designs, where the main limbs, yokes and any outer limbs are held together with core tie bolts. The severity of the losses encountered in a particular bolt will be therefore influenced by its location in the core and determined by the state of the local core saturation. The concept of the space-averaged permeability enables attention to be focused on the most susceptible regions of the core.

6.2 Topological calculation of flux variation

Fig. 9 also illustrates the flux density and flux line distribution in the core section surrounding the bolts, at the instant of the worst saturating conditions. It is revealed that the flux leaking into the bolt during a core saturation condition is concentrated at the outer surface, demonstrating the skin effect.

The illustration confirms that the worst condition is experienced by bolt B (in the main limb area).When the core is saturated, localised leakage of flux into the core bolt will give rise to eddy current heating of the bolt which will, in turn, heat the core bolt insulation, possibly causing deterioration over time and an eventual core short-circuit. For bolt A (in the yoke area), even though the core around the bolt is partially saturated, the bolt is still partly screened by the core. This is evident by the wider spread of flux lines around the core hole. As a mitigation action, the material for core bolts can be changed from magnetic to non-magnetic material since magnetic core bolts constitute the worst case in terms of eddy current induced overheating.

For the illustrations in Fig. 9, the individual bolts were represented explicitly in the finite-element model. However, to include all the core bolts in the model would result in a very large mesh (and long solution times) because it would be necessary to create a finite-element mesh adequate to model the electromagnetic skin effect in each bolt.

It may be noted, however, that the eddy currents induced in a bolt do not influence the overall flux distribution in the core. This observation leads to an alternative approach in which the time-domain solution is used to find the overall flux levels in the core (with the bolts ignored) and then, from this distribution, a time-varying boundary condition is obtained for a finite-element micromodel consisting of an individual bolt and the core region around it [27]. A subsequent thermal investigation may be performed as detailed in [27]; however, the temperature reached by the bolt will be critically dependent upon the local cooling of the core in the region of the core bolt and this is, presently, unknown.

Nevertheless, the use of the space-averaged core permeability variation can be used to focus attention on the bolts in the areas of highest saturation. Consequently, the specific objective of the second benchmarking concept is to calculate the flux conditions at the micromodel boundaries selected. For this, the following are noted: in a 2D finite-element formulation, the vector magnetic potential $\boldsymbol{A}$ behaves as a scalar quantity (two of the three components of the vector being explicitly zero) and a line of constant potential is a flux line. In addition, the difference in vector potential ($\boldsymbol{A}$) between any two points (A_1, A_2) is the flux (Φ) crossing a line joining them as given in (5).

$$\Phi = \int_{x_1}^{x_2} By \cdot \mathrm{d}x = \int_{x_1}^{x_2} -\frac{\partial \boldsymbol{A}}{\partial x} \cdot \mathrm{d}x = -A_2 + A_1 = (A_1 - A_2)\ \text{per\_m} \tag{5}$$

This observation may be used to establish the boundary

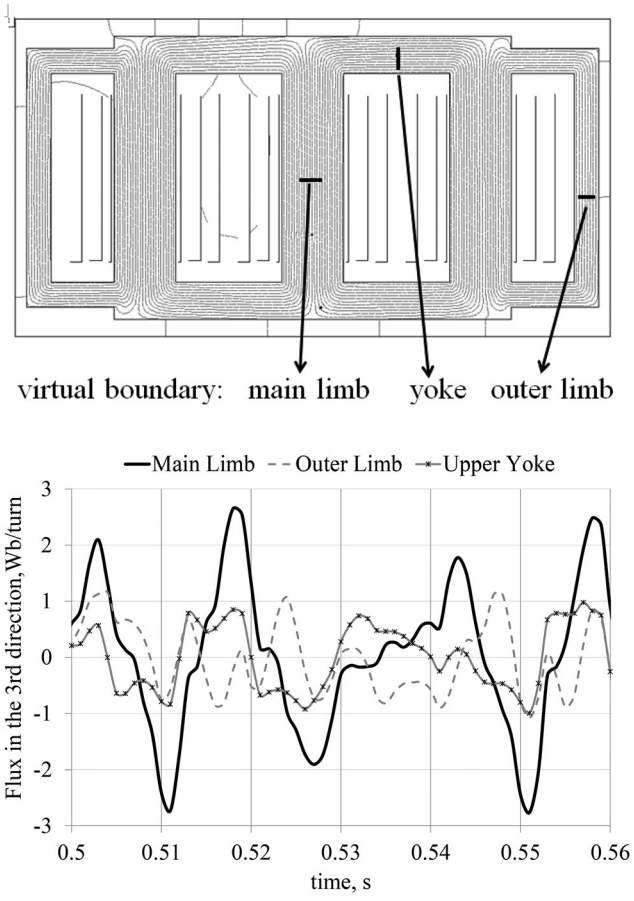

Fig. 11 *Flux variation at virtual boundaries*

conditions in the micromodel – two of which are set parallel to the flux direction (and are, therefore, flux lines) and two of which are set perpendicular to the flux flow. The micromodel is, thus, fluxed from its boundaries. Fig. 11 illustrates the flux variation monitored at three virtual boundaries located at the main limb, the yoke and the outer limb.

It can be seen that the flux variation in the main limb shows a much larger variation than that in at the other two locations, and so would be expected to give rise to higher losses in any core bolt present.

The simple post-processing operation described above allows a more detailed, localised and computationally affordable calculation of the flux variation at any number of virtual boundaries imposed on the core (e.g. within the main limb/yoke mitre zone), all from the single finite-element time-domain ferroresonance simulation. From this assessment, the most severe conditions can be selected for further study. Consequently, the susceptibility of the different parts of the core towards sustained ferroresonance can be assessed through Figs. 9 and 11.

It can be stated that in a five limb structure, the most susceptible parts of the core are, in order of severity, the main limbs, followed by the outer limbs and then the yokes. This is attributed to the fact that there is considerable flux leakage when the core is highly saturated, which means that it is only the parts of the core that are enclosed by the windings that will see the full flux. Furthermore, as is evident from Fig. 11, the peak flux reached by the yoke area is maintained at these high levels for longer time. On a final note, the flux in the outer limb area reaches its peak value on a more frequently than the flux variation in the main limbs.

7 Conclusions

This paper describes an autonomous modelling approach to assess, in the time domain, a power transformer under ferroresonance conditions through the integration of an external electrical circuit with a finite-element model. The methodology has the advantage over an equivalent circuit-based model of ferroresonance in that it can provide visual evidence of the core saturation, topologically, and allows examination of the core in detail for areas where local saturation may cause a problem.

For this, two benchmarking concepts were used; (i) the space-averaged permeability variation and (ii) a topological calculation of flux variation within the core. Through these concepts, the susceptibility of the different parts of the core towards sustained ferroresonance was determined. It was deduced that the most susceptible parts of a five limb core are, in order of severity, the main limbs, outer limbs and the yokes.

It is highlighted that under the method described, the finite-element equations and the circuit equations are solved simultaneously (not in some form of iterative loop) which renders the modelling process very simple and sequential. It is then possible to focus attention on such details as the eddy current heating of the most vulnerable of the core tie bolts, a consequence of which can be a failure of the bolt insulation leading to internal short-circuits in the core.

8 Acknowledgment

The technical and financial support provided by National Grid UK is acknowledged. Thanks to Alstom Grid Power Transformers for supplying details of the autotransformer design used in the modelling.

9 References

1 Tong, Y.K.: 'NGC experience on ferroresonance in power transformers and voltage transformers on HV transmission systems, warning! Ferroresonance can damage your plant'. IEE Colloquium, 12 November 1997
2 'Ferroresonance Tests on Brinsworth-Thorpe Marsh 400 kV circuit'. Technical Report TR (E) 389, Issue 1, National Grid, UK, July 2001
3 Mukerjee, R.N., Tanggaselu, B., Ariffin, A.E., Balakrishnan, M.: 'Indices for ferroresonance performance assessment in power distribution network'. Int. Conf. Power Systems Transients 2003 (IPST 2003), New Orleans, 2003, pp. 1–5
4 Jacobson, D.A.N., Menzies, R.W.: 'Investigation of station service transformer ferroresonance in Manitoba hydro's 230 kV Dorsey converter station'. Int. Conf. Power Systems Transients 2001 (IPST 2001), Rio de Janeiro, 24–28 June 2001, pp. 1–6
5 Slow Transients Task Force of the IEEE Working Group on Modeling and Analysis of Systems Transients Using Digital Programs: 'Modeling and analysis guidelines for slow transients – Part III: the study of ferroresonance', *IEEE Trans. Power Deliv.*, 2000, **13**, (1), pp. 255–265
6 Tran-Quoc, T., Pierrat, L.: 'An efficient non-linear transformer model and its application to ferroresonance study', *IEEE Trans. Magn.*, 1995, **31**, (3), pp. 2060–2063
7 Walling, R.A., Barker, K.D., Compton, T.M., *et al.*: 'Ferroresonant overvoltages in grounded Wye-Wye padmount transformers with low-loss silicon-steel cores', *IEEE Trans. Power Deliv.*, 1993, **8**, (3), pp. 1647–1660
8 Milicevic, K., Emin, K.Z.: 'Initiation of characteristic ferroresonance states based on flux reflection model', *IEEE Trans. Circuits Syst. Express Briefs*, 2013, **60**, (1), pp. 51–55
9 Rezaei-Zare, A., Iravani, R., Sanaye-Pasand, M., Mohseni, H., Farhangi, S.: 'An accurate hysteresis model for Ferroresonance analysis of a transformer', *IEEE Trans. Power Deliv.*, 2008, **23**, (3), pp. 1448–1456
10 Yunge, L., Shi, W., Furong, L.: 'Novel analytical solution to fundamental ferroresonance – Part I: power frequency excitation characteristic', *IEEE Trans. Power Deliv.*, 2006, **21**, (2), pp. 788–793
11 Moses, P.S., Masoum, M.A.S., Toliyat, H.A.: 'Impacts of hysteresis and magnetic couplings on the stability domain of ferroresonance in asymmetric three-phase three-leg transformers', *IEEE Trans. Energy Convers.*, 2011, **26**, (2), pp. 581–592
12 Reece, A.B.J., Preston, T.W.: 'Finite element methods in electrical power engineering' (Oxford University Press, 2000), pp. 16–25
13 Dreher, T., Meunier, G.: '3D modeling of electromagnets fed by alternating voltage sources', *IEEE Trans. Magn.*, 1993, **29**, (2), pp. 1341–1344
14 Renyuan, T., Shenghui, W., Yan, L., Xiulian, W., Xiang, C.: 'Transient simulation of power transformers using 3D finite element model coupled to electric circuit equations', *IEEE Trans. Magn.*, 2000, **36**, (4), pp. 1417–1420
15 Bouissou, S., Piriou, F.: 'Numerical simulation of a power transformer using 3D finite element method coupled to circuit equation', *IEEE Trans. Magn.*, 1994, **30**, (5), pp. 3224–3227
16 Charalambous, C.A., Wang, Z.D., Jarman, P., Osborne, M.: 'Core structure and its association with transformer susceptibility towards ferroresonance'. Int. Conf. Power Systems Transients (IPST2009), Kyoto, Japan, 3–6 June 2009
17 Charalambous, C., Wang, Z., Osborne, M., Jarman, P.: 'Sensitivity studies on power transformer ferroresonance of a 400 kV double circuit', *IET Proc. Gener. Transm. Distrib.*, 2008, **2**, (2), pp. 159–166
18 SLIM version 3.9.1 ©, ALSTOM GRID October 2013, support. slim@alstom.com
19 Charalambous, C., Wang, Z., Osborne, M., Jarman, P.: 'Validation of a power transformer model for Ferroresonance with system tests on a 400 kV circuit'. Int. Conf. Power Systems Transients 2007 (IPST 2007), Lyon, France, 4–7 June 2007
20 Watson, N., Arrillaga, J.: 'Power systems electromagnetic transient simulation', IEE Power Energy Series 39, 2003, The Institution of Electrical Engineers, 2003
21 Umenei, A.E., Melikhov, Y., Jiles, D.C.: 'Models for extrapolation of magnetization data on magnetic cores to high fields', *IEEE Trans. Magn.*, 2011, **47**, (12), pp. 4707–4711
22 Tang, Q., Wang, Z.D., Jarman, P.: 'Electrical steels and power transformer cores in deep saturation'. 2012 Int. Conf. Condition Monitoring and Diagnosis (CMD), 23–27 September 2012, pp. 1035–1038

doi: 10.1049/iet-epa.2013.0330

23 Sitzia, A.: 'The relationship between winding flux linkage and average vector potential, in SLIM Magnetic Solvers'. Technical Note – SLIM Technical Manual, ALSTOM Research and Technology, Stafford, UK, 13 September 2005
24 Sitzia, A.: 'Stacking factors and directional permeabilities in SLIM magnetic solvers'. Technical Note – SLIM Technical Manual, ALSTOM Research and Technology, Stafford, UK, 13 September 2005
25 Charalambous, C.A., Wang, Z.D., Jarman, P., Osborne, M.: 'Two dimensional finite element electromagnetic analysis of an auto-transformer experiencing ferroresonance', *IEEE Trans. Power Deliv.*, 2009, **24**, pp. 1275–1283
26 Charalambous, C.A., Wang, Z.D., Jarman, P., Sturgess, J.P.: 'Frequency domain analysis of a power transformer experiencing sustained ferroresonance', *IET Gener. Transm. Distrib.*, 2011, **5**, (6), pp. 640–649
27 Charalambous, C.A., Zhang, R., Wang, Z.D.: 'Simulating thermal conditions around core bolts when transformer is experiencing ferroresonance'. Paper number 211, I.P.S.T, Netherlands 2011, Delft, The Netherlands, 14–17 June 2011